Novel unimorph deformable mirror for solid state laser resonators

S. Verpoort*, P. Welp, and U. Wittrock
[a]Muenster University of Applied Sciences, Photonics Laboratory, Stegerwaldstr. 39,
48565 Steinfurt, Germany

ABSTRACT

We present a novel unimorph deformable mirror with a diameter of only 10 mm that will be used in adaptive resonators of high power solid state lasers. The relationship between applied voltage and deformation of a unimorph mirror depends on the piezoelectric material properties, layer thicknesses, boundary conditions, and the electrode pattern. An analytical equation for the deflection of the piezoelectric unimorph structure is derived, based on the electro-elastic and thin plate theory. The validity of the proposed analytical model has been proven by numerical finite-element modelling and experimental results. Our mirror design has been optimized to obtain the highest possible stroke and a high resonance frequency.

1. INTRODUCTION

One of the key interests in developing lasers is the achievement of a high brightness, i.e. high output power and high beam quality at the same time. The radial temperature profile in the gain medium of a high-power solid state laser will always differ from the ideal parabolic temperature profile, leading to aberrations. The deviation from an ideal parabolic profile is due to many effects, such as an inhomogeneous heating and/or cooling of the laser crystal, or the temperature dependence of the heat conductivity. Since the early 1970s, scientists tried to enhance the beam quality and laser efficiency by the use of deformable mirrors in order to compensate the optical aberrations of the thermal lens [1]. This requires a deformable mirror which is capable of handling high power. Currently, adaptive optics has mostly been used in high-power laser amplifiers. While this approach has proven its utility it would be very useful to employ adaptive optics also directly in the resonator of high-power lasers. This requires smaller mirrors because typical beam diameters are of the order of a few millimeters only and it would often be impractical to employ intracavity beam expanders.

2. UNIMORPH MIRROR FOR HIGH POWER LASER SYSTEMS

The key element for the intracavity aberration compensation in solid state lasers is the deformable mirror. Intracavity correction requires adaptive correctors with high damage threshold and sufficient stroke. At the same time, the mirror needs to have a sufficient actuator density underneath the beam footprint. Furthermore, a small diameter of the mirror is desirable due to the extreme sensitivity of laser resonators with large fundamental-mode diameters to aberrations. There is a wide variety of commercially available adaptive mirrors, but neither meets all requirements. In this paper we present a novel adaptive mirror based on the unimorph principle which can fulfill these requirements. The unimorph design should enable a dynamic compensation for low- and medium-order optical aberrations. A unimorph mirror has the advantage that it does not suffer from print-through of the actuators because the passive layer equalizes local deformations. Actuator print-through is sometimes encountered in bimorph mirrors and in membrane mirrors and leads to aberrations of high spatial frequencies. This can result in unwanted hotspots during beam propagation. Unimorph mirrors can be fabricated with superpolished optical glass as the passive layer. Such glasses can be furnished with sputtered dielectric multi-layer coatings that yield very high reflectivity, as well as low scattering and absorption. This is a prerequisite for the use of these mirrors in high-average-power lasers.

MEMS Adaptive Optics III, edited by Scot S. Olivier, Thomas G. Bifano, Joel A. Kubby, Proc. of SPIE
Vol. 7209, 72090N · © 2009 SPIE · CCC code: 0277-786X/09/$18 · doi: 10.1117/12.810135

2.1 Analytical Modelling

This section investigates the mechanical behavior of a circular piezoelectric unimorph mirror with an unsegmented electrode. Such a mirror would be of limited use in a laser because it can only compensate defocus aberrations, but its analysis provides important guidelines for designing unimorph mirrors with segmented electrodes that can compensate higher-order aberrations. In order to investigate the effects of several critical design parameters, an analytical equation for analyzing the deflection of the unimorph piezoelectric structure is derived, based on the electro-elastic theory and Kirchhoff´s thin plate theory. The validity of the proposed analytical model is further studied by using the COMSOL Multiphysics finite element method (FEM) software package. Piezoelectric actuators consisting of a piezoelectric (active) layer bonded to a non-piezoelectric (passive) elastic layer are widely used in micro-electro-mechanical systems (MEMS). Several simple analytical and numerical models have been proposed for symmetrical structures that consist of a piezoelectric layer and a passive layer that have equal thicknesses. However, there are only a few publications dealing with structures where the layer-thicknesses are different and most of these describe their models in Cartesian coordinates which is not suitable for our purposes [3, 4]. In [5] the authors consider the case of unimorph actuators with different geometric shapes. The calculations are carried out in Cartesian coordinates as well as in cylindrical coordinates. However, the equation for the displacement of circular unimorph structures they derive seems to be incorrect, because they omit the scaling factor $1/(1-\nu)$ in the equation for the piezoelectric induced bending moment.

The following calculations have been performed in cylindrical coordinates. A circular unimorph structure is shown in Fig. 1a. The structure consists of a piezoelectric disc sandwiched between two metallic electrodes, a bonding layer and a passive disc. In our case, the passive disc is a thin disc of high-quality optical glass. The piezoelectric disc is glued onto the passive glass disc by the bonding layer. As the bonding layer and the electrodes are very thin compared to the overall thickness of the unimorph structure, they are neglected in our model. Consider a unimorph consisting of a piezoelectric disc of thickness h_p and Young´s modulus E_p and a glass disc (non-piezoelectric) of thickness h_{np} and Young´s modulus E_{np}. Figure 1b shows the cross section of this laminate structure. When a voltage is applied to the piezo disc, the piezoelectric element strains azimuthally and radially due to the reverse piezoelectric effect. For the reverse piezoelectric effect, the strain is proportional to the piezoelectric coefficient d_{31}. The different relative strains of the glass disc and the piezo disc result in lateral stress between the two discs causing the laminate to deform into a spherical surface. The transverse displacement per unit voltage obtained by such a unimorph structure (flextensional mode) is typically much greater than that of the bulk piezoelectric material (extensional mode). The total thickness of the unimorph and the thickness ratio between the piezoelectric disc and the non-piezoelectric disc affect the total displacement.

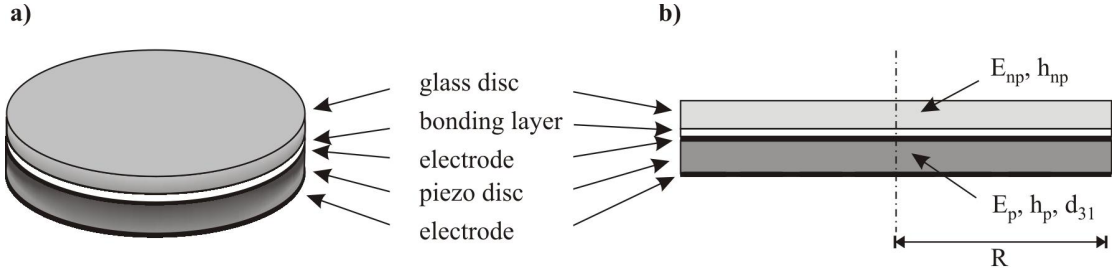

Fig. 1: a) Three-dimensional view of a simple unimorph structure, b) corresponding cross sectional view.

The following calculations are based on the Kirchhoff's hypotheses of classical thin plate theory [6, 7]:

- the individual layers are perfectly bonded, i.e. there are no displacements of the layers relative to each other
- straight lines originally perpendicular to the plate's middle plane remain straight and perpendicular even after deformation ("normals remain straight and normal")
- lines normal to the large surfaces of the discs keep the same length ("normals remain unstretched")

2.2 Bending of a simply supported homogeneous circular disc

Before analyzing the two-layer laminate that we described in the last paragraph, we consider a single-layer homogeneous circular disc that is supported along its rim. The position of the rim shall be kept fixed, but rotation of the disc's volume elements at the rim shall be allowed. We neglect gravitational forces and these support conditions are therefore represented by vanishing external bearing forces F_L and bearing moments M_L along the rim. We follow the convention in plate theory and use forces and moments per unit length acting around the circumference instead of total forces and total moments. Furthermore we assume that an external bending moment $m_r(R) = m_0$ acts on the rim of the disc. If the disc bends due to the action of this moment, points initially located at some distance from the center are shifted radially by $w_r = z \cdot \varphi$ (see Fig. 2c), where φ is the local slope of the disc´s surface.

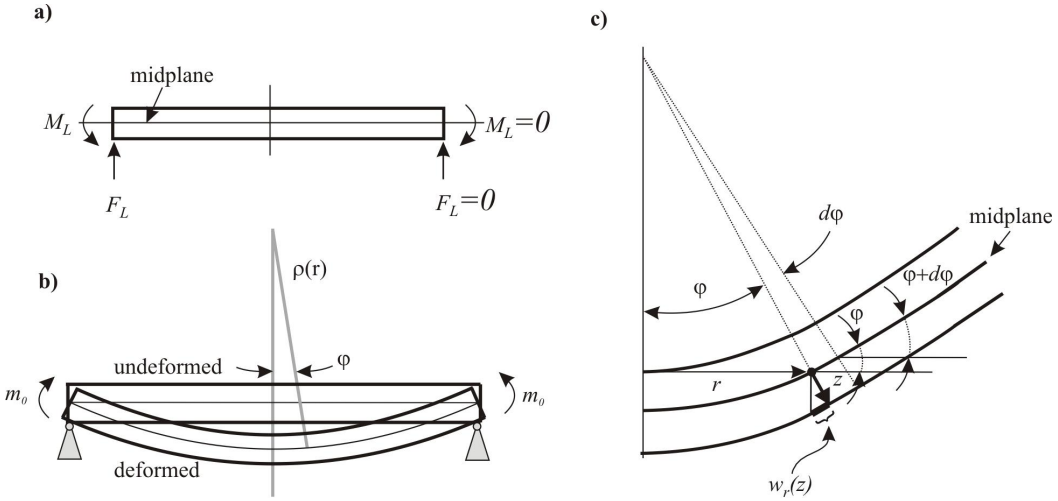

Fig. 2: a), b) Definition of the boundary conditions, c) meridional cross section showing the radial displacement $w_r(z)$ of a point on the surface of the disc.

These displacements w_r lead to radial and tangential strains which are given by

$$s_r = \frac{dw_r}{dr} = \frac{d\varphi}{dr} \cdot z \tag{1.1}$$

$$s_t = \frac{w_r}{r} = \frac{\varphi}{r} \cdot z \tag{1.2}$$

For the considered case of plane stress the following applies:

$$s_r = \frac{1}{E}\left(T_r - \nu \cdot T_t\right) \tag{1.3}$$

$$s_t = \frac{1}{E}\left(T_t - \nu \cdot T_r\right) \tag{1.4}$$

where E is the Young's modulus of the disc, ν is the Poisson ratio, and T_r, T_t are the resulting tangential and radial stresses. The stresses are now determined by

$$T_r = \frac{E}{1-\nu^2}\left(\frac{d\varphi}{dr} + \nu \cdot \frac{\varphi}{r}\right) \cdot z \tag{1.5}$$

$$T_t = \frac{E}{1-\nu^2}\left(\frac{\varphi}{r} + \nu \cdot \frac{d\varphi}{dr}\right) \cdot r \tag{1.6}$$

Figure 3 shows a volume element of the plate $\left(r \cdot d\alpha \cdot dr \cdot h\right)$ bounded by radial and meridional sections.

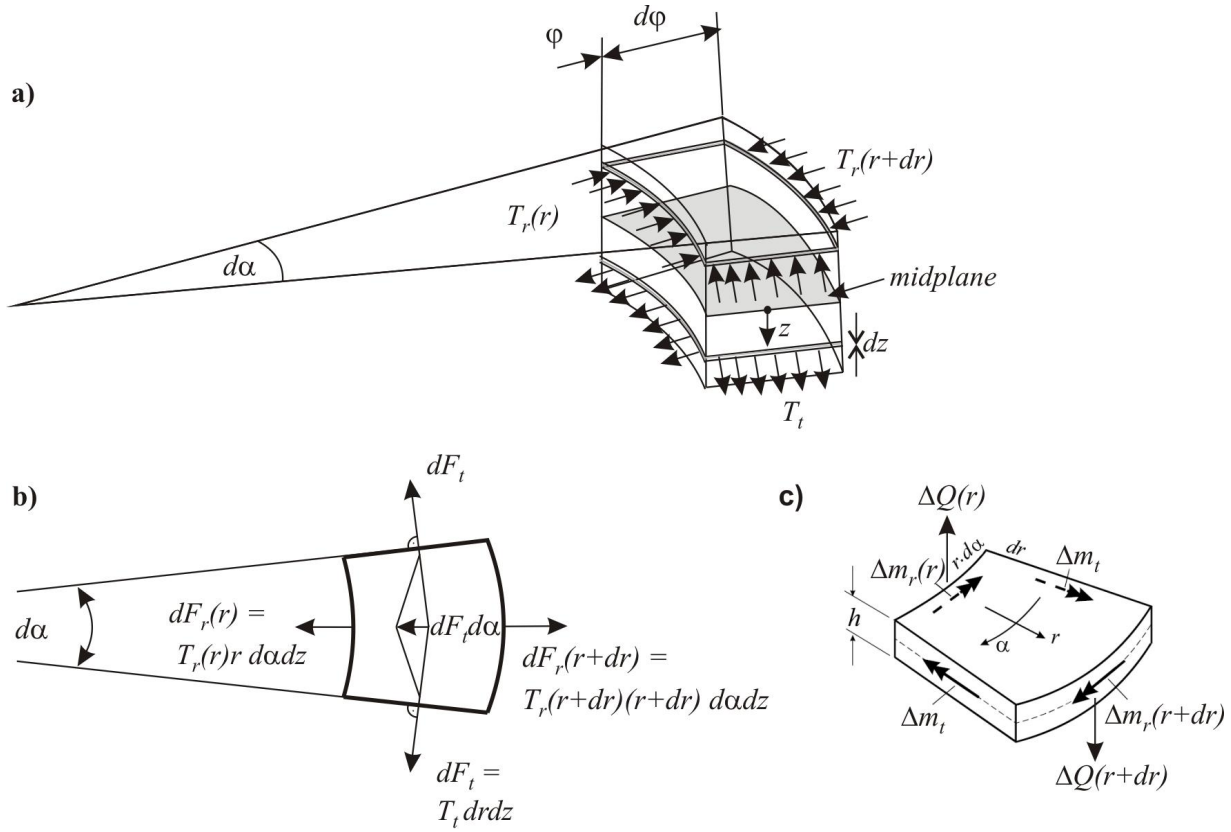

Fig. 3: Balance of moments of a volume element: a) stresses at the sections, b) stress resultants of a volume element with height *dz*, c) moments and shearing forces at the sections.

For $z > 0$ the fibers are strained radially as well as tangentially, i.e. $s_r > 0$ and $s_t > 0$. The bending moments per unit length can be calculated according to

$$\begin{aligned}
\Delta m_r(r) &= \int_{-h/2}^{h/2} z \cdot T_r(r) \cdot dz \\
\Delta m_r(r+dr) &= \int_{-h/2}^{h/2} z \cdot T_r(r+dr) \cdot dz \\
&= \int_{-h/2}^{h/2} z \cdot \left[T_r(r) + dT_r(r)\right] \cdot dz \\
&= \Delta m_r(r) + \int_h dT_r(r) \cdot z \cdot dz \\
\Delta m_t &= \int_{-h/2}^{h/2} z \cdot T_t(r) \cdot dz
\end{aligned} \tag{1.7}$$

Here, the two tangential moments of each volume element assume such a value that the meridional sections remain straight. The moments subtend an angle $d\alpha$ and their vector addition $\Delta m_{t,res} = \left|\Delta \vec{m}_t(\alpha) + \Delta \vec{m}_t(\alpha + d\alpha)\right| = \Delta m_t(a) \cdot d\alpha$ leads to a moment with the same rotation direction as $\Delta m_r(r)$. The balance of moments can be obtained as

$$\Delta m_r(r+dr) - \Delta m_r(r) - \Delta m_t \cdot d\alpha = 0 \tag{1.8}$$

By substitution of equations (1.5) and (1.6) into equation (1.7), the bending moments can be expressed by

$$m_r = D\left(\frac{d\varphi}{dr} + \nu \cdot \frac{\varphi}{r}\right) \tag{1.9}$$

$$m_t = D\left(\frac{\varphi}{r} + \nu \cdot \frac{d\varphi}{dr}\right) \tag{1.10}$$

where the flexural rigidity of the plate D is defined by

$$D = \int_{-h/2}^{h/2} \frac{E}{1-\nu^2} \cdot z^2 \cdot dz = \frac{E \cdot h^3}{12 \cdot \left(1-\nu^2\right)} \tag{1.11}$$

Substitution of equations (1.9) and (1.10) in (1.8) yields the homogeneous differential equation for the bending angle

$$\frac{d^2\varphi}{dr^2} + \frac{1}{r}\frac{d\varphi}{dr} - \frac{\varphi}{r^2} = \frac{d}{dr}\left[\frac{1}{r} \cdot \frac{d(r \cdot \varphi)}{dr}\right] = 0 \tag{1.12}$$

The solution is given by

$$\varphi_{\text{hom}} = C_1 \cdot r + \frac{C_2}{r} \tag{1.13}$$

For massive plates, C_2 is always zero because of the singularity of φ for $r \to 0$. The constant C_1 can be obtained by the boundary conditions. In case of an external moment $m_r(R) = m_0$ acting on the rim and vanishing bearing moments, the displacement in the center of the disc can be calculated from the following equation

$$m_r = D \cdot \left(\frac{d\varphi}{dr} + \nu \cdot \frac{\varphi}{r}\right) = D \cdot C_1\left(1+\nu\right) \tag{1.14}$$

From Eq. (1.14) we obtain the bending angle $\varphi(r)$, the deflection $h(r)$, and the total deflection $h_{\max} = h(R)$.
(see Fig. 4a):

$$\varphi(r) = \frac{m_0}{\left(1+\nu\right) \cdot D} \cdot r \tag{1.15}$$

$$h(r) = \int_0^r \varphi(r)\, dr = \frac{m_0}{2\left(1+\nu\right) \cdot D} r^2 \tag{1.16}$$

$$\begin{aligned} h_{\max} = h(R) &= \frac{R^2}{2 \cdot \left(1+\nu\right) \cdot D} \cdot m_0 \\ &= \frac{6\left(1-\nu\right)R^2}{E \cdot h^3} \cdot m_0 \end{aligned} \tag{1.17}$$

2.3 Unimorph two-layer laminate

After the treatment of the single-layer homogeneous disc subjected to an external bending moment, we consider the unimorph two-layer laminate consisting of a piezoelectric disc bonded to a passive disc (see Fig. 1b). When a voltage is applied to the piezo disc, a piezoelectric internal bending moment m_{piezo} is being induced. This moment is equivalent to a bending moment m_0 acting along the rim. As a result, the two-layer laminate bends around its neutral axis, i.e. the plane inside the laminate that does not show transverse or radial strain. In order to calculate the deformation of the two-layer laminate with different Poisson ratios we have to calculate a weighted mean value for the whole structure which is defined by [8]:

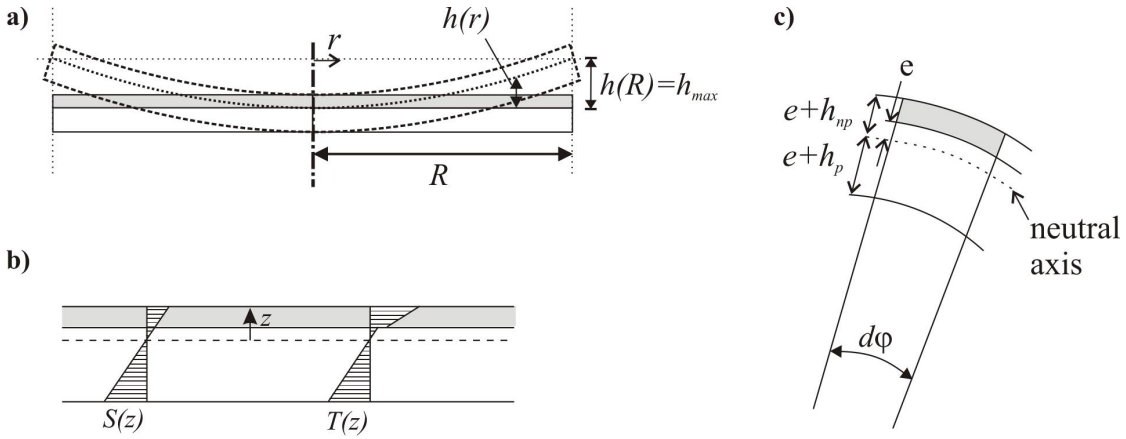

Fig. 4: The two-layer laminate: a) deflection *h(r)* depending on the radial position, b) cross section showing the stress and strain distribution of the laminate, c) location of the neutral axis.

$$\nu_{weighted} = \int_h \frac{\nu(z)\cdot E(z)}{1-\nu(z)^2}dz \cdot \left[\int_h \frac{E(z)}{1-\nu(z)^2}dz\right]^{-1} = \frac{\nu_p + \nu_{np}(a\cdot b\cdot \beta)}{1+(a\cdot b\cdot \beta)}, \tag{1.18}$$

where $a = h_{np}/h_p$ is the relative thickness and $c = E_{np}/E_p$ is the relative elasticity of the non-piezoelectric material compared to the piezoelectric material and $\beta = (1-\nu_p)/(1-\nu_{np})$. Under outer bending the strain is proportional to the distance from the neutral axis, whereas the location of the neutral axis is characterized by the distance *e* to the interface between the two layers (see Fig. 4c). The stresses make a step at the interface according to the different Young's moduli as shown in Fig. 4b:

$$T_{r,p} = \frac{E_p}{1-\nu^2}\left(\frac{d\varphi}{dr} + \nu\cdot\frac{\varphi}{r}\right)\cdot z \qquad e-h_p \le z \le e \tag{1.19}$$

$$T_{r,np} = \frac{E_{np}}{1-\nu^2}\left(\frac{d\varphi}{dr} + \nu\cdot\frac{\varphi}{r}\right)\cdot z \qquad e \le z \le e+h_{np} \tag{1.20}$$

Because of the balance of the radial stresses

$$\int_h T_r\cdot dz = \frac{1}{1-\nu^2}\left(\frac{d\varphi}{dr} + \nu\cdot\frac{\varphi}{r}\right)\cdot\left[E_p\int_{e-h_p}^{e} z\cdot dz + E_{np}\int_e^{e+h_{np}} z\cdot dz\right] = 0 \tag{1.21}$$

the distance *e* is given by

$$e = \frac{E_p h_p^2 - E_{np}h_{np}^2}{2\left(E_p h_p - E_{np}h_{np}\right)} = \frac{h_p}{2}\frac{1-a^2\cdot c}{1+a\cdot c} \tag{1.22}$$

Now, with the known location of the neutral axis, we can calculate the inner moments which balance the outer moments

$$\begin{aligned} m_r &= \int_h z\cdot T_r\cdot dz = \frac{1}{1-\nu^2}\left(\frac{d\varphi}{dr} + \nu\cdot\frac{\varphi}{r}\right)\cdot\left[E_p\int_{e-h_p}^{e} z\cdot dz + E_{np}\int_e^{e+h_{np}} z\cdot dz\right] \\ &= \left(\frac{d\varphi}{dr} + \nu\cdot\frac{\varphi}{r}\right)\cdot\frac{2}{3}\frac{E_p h_p^3}{\left(1-\nu^2\right)}\cdot\frac{4ac\left(1+a\right)^2 + \left(1-a^2c\right)^2}{8\left(1+ac\right)} \end{aligned} \tag{1.23}$$

Therefore, the flexural rigidity of the two-layer laminate is given by

$$D = \frac{2}{3}\frac{E_p h_p^3}{\left(1-\nu^2\right)} \cdot \frac{4ac\left(1+a\right)^2 + \left(1-a^2c\right)^2}{8\left(1+ac\right)} \tag{1.24}$$

The piezoelectric-induced bending moments caused by applying a voltage can be calculated under the condition of constrained deflection. At first, we consider the non-bonded two-layer system (see Fig. 5). On applying an electric field $\vec{E}$, the piezoelectric disc expands and the radius changes by $\Delta R = d_{31} \cdot \left|\vec{E}\right| \cdot R$. If we apply radial tensile stress on the glass disc and radial compressive stress on the piezo disc that correspond to identical absolute forces, the radii of the discs are forced to be equal. This stress condition results in a displacement $w_r = w_{r,np}$ in the non-piezoelectric disc and $w_{r,p} = -d_{31} \cdot E \cdot R + w_{r,np}$ in the piezo disc. If we consider the equilibrium condition $T_{r,np} \cdot h_{np} + T_{r,p} \cdot h_p = 0$, we obtain

$$T_{r,np} = \frac{E_{np}}{1-\nu} \cdot \frac{w_{r,np}}{R} = \frac{E_{np}}{1-\nu} \cdot d_{31} \cdot \left|\vec{E}\right| \cdot \frac{1}{1+ac} \tag{1.25}$$

$$T_{r,p} = -\frac{E_p}{1-\nu} \cdot d_{31} \cdot \left|\vec{E}\right| \cdot \frac{ac}{1+ac} = -a \cdot T_{r,np} \tag{1.26}$$

When the two discs are bonded together, their stress condition does not change. The stress components $T_{r,p}$ and $T_{r,np}$ remain the same. The generated bending moment can be calculated according to

$$m_{piezo} = m_0 = \int_{e-h_p}^{e+h_{np}} T_r(z) \cdot z \cdot dz = h_p^2 \cdot d_{31} \cdot \left|\vec{E}\right| \cdot \frac{E_p}{1-\nu} \frac{ac\left(1+a\right)}{2\left(1+ac\right)} \tag{1.27}$$

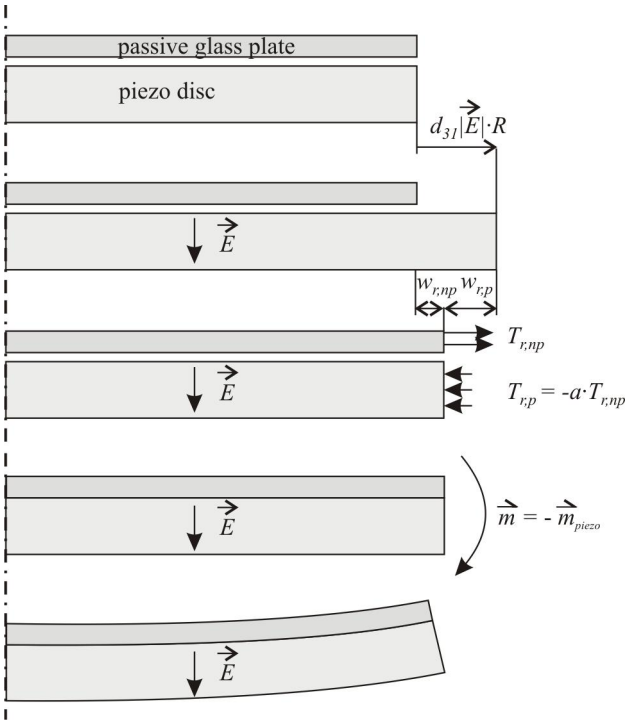

Fig. 5: This schematic illustrates the logical steps of the model for a unimorph mirror with a single electrode. First, we consider the free expansion of the piezo disc if a voltage is applied. Then, we constrain the lateral expansion by glueing the piezo and glass discs together, but prevent bending by applying artificial external stresses *T* or an artificial external moment *m*. Finally, we remove this artificial external influence and let the mirror deform.

At this point, we can calculate the maximum displacement $h_{\max}(R)$ of the circular unimorph by substitution of equation (1.27) and equation (1.24) into equation (1.17):

$$h_{\max}(R) = \frac{m_{piezo} \cdot R^2}{2(1+\nu)D} = \frac{4ac(1+a)}{4ac(1+a)^2 + (1-a^2c)^2} \frac{h_p^2 \cdot d_{31} \cdot |\vec{E}| \cdot E_p}{1-\nu} \cdot \frac{R^2}{2(1+\nu)} \cdot \frac{3(1-\nu^2)}{2 \cdot E_p \cdot h_p^3} \tag{1.28}$$

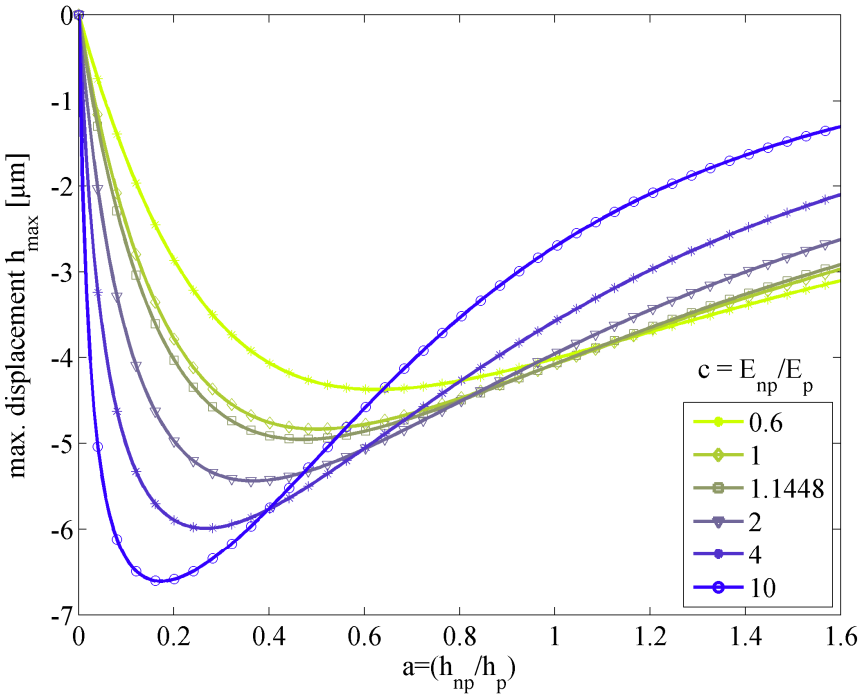

Fig. 6: Maximum displacement as a function of the thickness ratio of the passive disc and the piezo disc. Several curves for different ratios *c* of the Young's moduli are shown.

3. EXPERIMENTAL RESULTS

The analytical equation (1.28) derived in the previous section allows to directly predict the performance of the piezoelectric unimorph mirror depending on material properties and the dimensions of the individual layers. However, such an analytical solution needs to be verified since the derivation process involves the major assumption of strain distributions within the piezo disc, the bonding adhesive, and the passive layer that are linear in *z* (see Fig. 4b). One effective way to verify this analytical solution is to compare it with results from an FEM simulation. We used the commercial FEM package Comsol Multiphysics 3.4. The mesh generation was developed in the Comsol mesh generator using Lagrange Quadratic Tetrahedral elements. Our FEM model contains approximately 11000 mesh elements. Another way to verify the final equation (1.28) is to compare its results with available experimental data. For the experiment, we fabricated several unimorph mirrors with unsegmented electrodes. All mirrors had identical passive disc thicknesses but various piezo disc thicknesses. The properties of the piezo disc, the adhesive and the passive glass discs are summarized in the following table.

Table 1: The material properties and dimensions which we used in our analytical and numerical models as well as for the unimorph mirrors which we manufactured.

Component	**Property**	**tensor (in order of x, y, z, xy, yz, and xz) / value**
piezo disc	piezoelectricity $\boldsymbol{e}$ (C m^{-2}) (stress-charge form)	$\begin{bmatrix} 0 & 0 & -7.15 \\ 0 & 0 & -7.15 \\ 0 & 0 & 13.70 \\ 0 & 0 & 0 \\ 0 & 11.90 & 0 \\ 11.90 & 0 & 0 \end{bmatrix}$
	relative permittivity $\boldsymbol{\varepsilon_T}$	$\begin{bmatrix} 1649 & 0 & 0 \\ 0 & 1649 & 0 \\ 0 & 0 & 1750 \end{bmatrix}$
	compliance $\boldsymbol{S}$ (m^2 N^{-1})	$\begin{bmatrix} 15.90 & -5.69 & -7.37 & 0 & 0 & 0 \\ -5.69 & 15.90 & -7.37 & 0 & 0 & 0 \\ -7.37 & -7.37 & 20.97 & 0 & 0 & 0 \\ 0 & 0 & 0 & 44.92 & 0 & 0 \\ 0 & 0 & 0 & 0 & 44.92 & 0 \\ 0 & 0 & 0 & 0 & 0 & 43.19 \end{bmatrix} \times 10^{-12}$
	disc thickness (μm)	experiments: 200, 500, 1000; calculations: 150 – 1400
	disc diameter (mm)	10
	Poisson ratio γ	0.36
	Young's modulus $\boldsymbol{E}$ (GPa)	62.9
	piezoelectric strain constant d_{31} (mV^{-1})	-174×10^{-12}
bonding layer	thickness (μm)	~ 10
	Young's modulus $\boldsymbol{E}$ (GPa)	~ 6
passive glass disc	disc diameter (mm)	10
	disc thickness (μm)	160
	Poisson ratio γ	0.208
	Young's modulus $\boldsymbol{E}$ (GPa)	72

The total deflection of a unimorph mirror with a glass thickness of 160 μm has been calculated from the analytical solution (1.28). The result is shown in Fig. 7 as a function of the thickness of the piezo disc. Also shown in Fig. 7 are the results of the FEM simulations and experimental results for three mirrors with glass thicknesses of 200 μm, 500 μm, and 1000 μm which we have built. The experimental and numerical data are in very good agreement with the analytical results. For the subsequent fabrication of our first prototype of a deformable, multi-actuator unimorph mirror with segmented electrodes we used commercially available piezo discs with a diameter of 10 mm and a thickness of 200 μm.

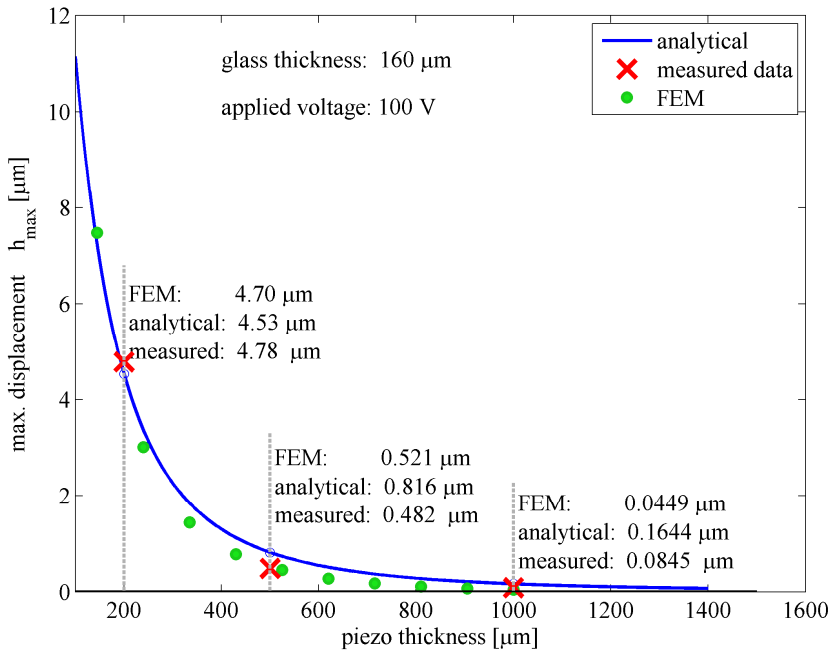

Fig. 7: Comparison of analytical, numerical and experimental data. Plotted is the total deflection of the mirror as a function of the piezo thickness for a glass thickness of 160 µm and an applied voltage of 100 V. Experimental results for piezo thicknesses of 200 µm, 500 µm, and 1000 µm are shown as well.

Our analytical equation (1.28) predicts an optimal passive plate thickness ratio of 0.47 for the given Young's modulus ratio of 1.14 for the piezo-glass combination and a piezo thickness of 200 µm. Therefore, we use fused silica glass discs of 100 µm thickness as passive plates for manufacturing our mirrors. These thicknesses of the piezo- and glass discs lead to a stroke of 4.7 µm at an excitation voltage of 100 V. On delivery, the commercial piezo discs already showed a very strong astigmatic peak-to-valley deformation of 24 λ_{HeNe} (632.8 nm) caused by the fabrication process. In order to achieve a sufficiently flat surface the discs had to be ground and lapped. During the grinding and lapping steps fabrication induced internal stresses of the piezo disc were released. This finally led to slightly spherically deformation. The fabricated mirrors had a peak-to-valley deformation of 1.87 λ_{HeNe} which was predominately defocus. The electrode pattern on the back side of the piezo discs consists of 17 sectors.

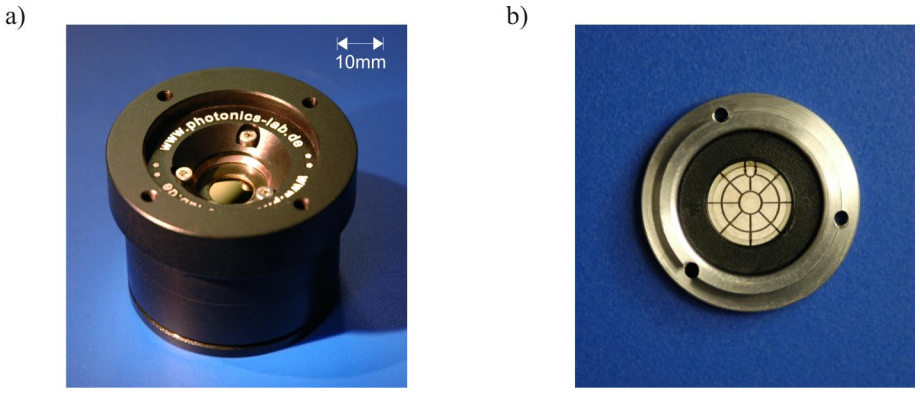

Fig. 8: First prototype of the unimorph mirror: a) The mirror mounted in its housing, b) the electrode pattern with 17 sectors.

The measured influence functions of the electrodes as well as the numerically simulated influence functions are shown in Fig. 9a and Fig. 9b. The calculated FEM surface profiles show a very good agreement with the measured ones. Therefore it should be possible to use the FEM model as a tool to further optimize the design of our adaptive mirror.

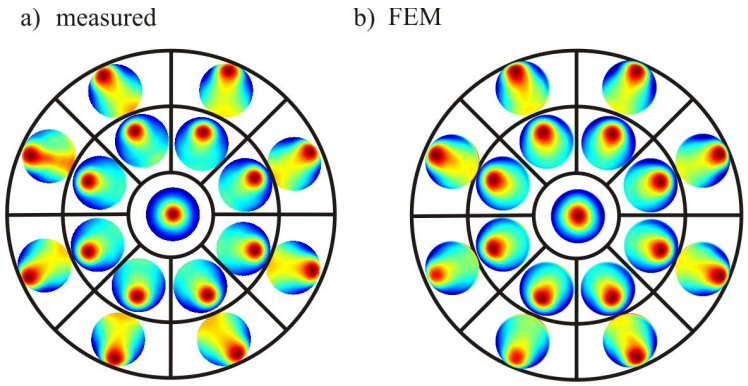

Fig. 9: This figure shows the influence functions of the different electrodes. Shown is the deformation that results if a single electrode is supplied with a voltage of 100 V. The false-color elevation plots that represent the mirror deformations are plotted at a position that corresponds to the electrode that is being activated. a) Experimentally measured influence functions of a fabricated mirror, b) FEM simulation of the influence functions.

In Fig. 10 we show the initial and the flattened surface of our first unimorph mirror, along with the corresponding interferograms. The surface could be flattened by actuating the electrodes in a feed-forward scheme. The surface deformation was reduced from 1.87 λ_{HeNe} peak-to-valley deformation and 0.45 λ_{HeNe} root-mean square (rms) deviation to 0.35 λ_{HeNe} peak-to-valley and 0.07 λ_{HeNe} rms. The active flattening is mainly limited by the voltage discretization of our high-voltage driver. The digital-analog converter (DAC) of the high-voltage driver allows to control up to 60 channels with a precision of only 6 bit over a voltage range of 300 V. This fact results in large voltage steps of 4.7 V. Therefore, for future experiments we will exchange the 6-bit DAC modules by new 12-bit high-resolution DAC modules.

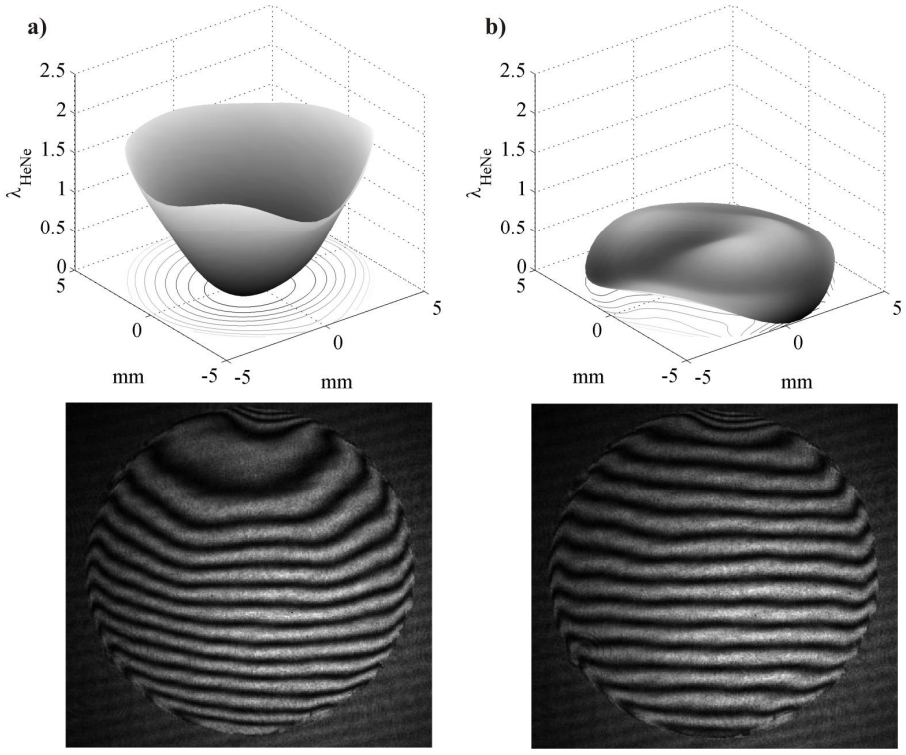

Fig. 10: Measured surface deformation of our first mirror. a) Zero voltage deformation, b) the flattened surface after suitable activation of the electrodes. The lower pictures show the measured interferograms, the upper pictures the surface shape that was derived from the interferograms.

4. FUTURE WORK

The next step in the development of our small-aperture adaptive unimorph mirrors for solid state laser resonators is to apply a high-reflection dielectric multi-layer coating onto the glass surface. A reflectivity in the range of 99.99 % should be achieved in order to ensure negligible thermal deformation of the adaptive mirror under laser load. Furthermore, the number of electrodes is to be increased in order to provide a higher actuator density. The electrode pattern will be optimized for optimum compensation of measured aberrations in high-power lasers. Static aberrations of the mirror surface will be further reduced by optimized fabrication procedures.

5. CONCLUSION

An analytical equation for the analysis of a piezoelectric unimorph mirror was derived, based on the assumption of a linear strain distribution in the piezo disc, the bonding layer, and the passive glass disc. Results from both FEM simulations as well as experimental data verified the validity of the analytical solution. By means of this equation the performance of the piezo-glass laminate structure can be predicted which allowed us to optimize the design. Based on the results gained from the analytical model and the FEM simulation a first prototype of a small diameter unimorph mirror with 17 sector electrodes has been built and characterized.

6. ACKNOWLEDGMENTS

The authors gratefully acknowledge partial support for this work by Thorlabs GmbH / Germany. Furthermore, we thank H. Franke at the University of Duisburg-Essen / Germany for providing technical support and valuable discussions.

REFERENCES

[1] Oughstun, K. E., "Intracavity adaptive optics compensation of phase aberrations," *J. Opt. Soc. Amer.* **71**, 862-872 (1981).
[2] Stephens, R. R. and Lind, R. C., "Experimental study of an adaptive-laser resonator," *Optics Letters* **3**, 79-81 (1978).
[3] Kudryashov, A. and Shmalhausen, V., "Semipassive bimorph flexible mirrors for atmospheric adaptive optics applications," *Opt. Eng.* **35** 3064-3073 (1996).
[4] Ellis, E. M. , "Low-cost bimorph mirrors in adaptive optics," Ph.D. thesis, University of London, (1999).
[5] Li, X., Shih, W. Y., "Electromechanical behavior of PZT-brass unimorphs," *J. Am. Ceram. Soc.* **82**, 1733-1740 (1999).
[6] Timoshenko, S. and Woinowsky-Krieger, S., "Theory of Plates and Shells," McGraw-Hill, New York (1959).
[7] Rogacheva, N. N., "Equation of state of piezoelectric shells," Prikl. Mat. Mekh. **11**, 5 (1981).
[8] Pfeifer, G., "Piezoelektrische Biegeelemente mit passiver Trägerplatte als Stellelemente für die Feinwerktechnik," Feingerätetechnik, **26**, 5 (1977).